doi:10.1016/j.jmb.2008.12.070 J. Mol. Biol. (2009) 386, 789–801

JMB

Available online at www.sciencedirect.com

ScienceDirect

ELSEVIER

HIV-1 Nucleocapsid Protein Switches the Pathway of Transactivation Response Element RNA/DNA Annealing from Loop–Loop "Kissing" to "Zipper"

My-Nuong Vo[1,2], George Barany[1,2], Ioulia Rouzina[3]* and Karin Musier-Forsyth[4,5]*

[1]*Department of Chemistry, University of Minnesota, Minneapolis, MN 55455, USA*

[2]*Institute for Molecular Virology, University of Minnesota, Minneapolis, MN 55455, USA*

[3]*Department of Biochemistry, Molecular Biology, and Biophysics, University of Minnesota, Minneapolis, MN 55455, USA*

[4]*Department of Chemistry, The Ohio State University, Columbus, OH 43210, USA*

[5]*Department of Biochemistry, The Ohio State University, Columbus, OH 43210, USA*

Received 30 August 2008; received in revised form 20 December 2008; accepted 29 December 2008
Available online 6 January 2009

Edited by J. Doudna

The chaperone activity of HIV-1 (human immunodeficiency virus type 1) nucleocapsid protein (NC) facilitates multiple nucleic acid rearrangements that are critical for reverse transcription of the single-stranded RNA genome into double-stranded DNA. Annealing of the transactivation response element (TAR) RNA hairpin to a complementary TAR DNA hairpin is an essential step in the minus-strand transfer step of reverse transcription. Previously, we used truncated 27-nt mini-TAR RNA and DNA constructs to investigate this annealing reaction pathway in the presence and in the absence of HIV-1 NC. In this work, full-length 59-nt TAR RNA and TAR DNA constructs were used to systematically study TAR hairpin annealing kinetics. In the absence of NC, full-length TAR hairpin annealing is ~10-fold slower than mini-TAR annealing. Similar to mini-TAR annealing, the reaction pathway for TAR in the absence of NC involves the fast formation of an unstable "kissing" loop intermediate, followed by a slower conversion to an extended duplex. NC facilitates the annealing of TAR by ~10^5-fold by stabilizing the bimolecular intermediate (~10^4-fold) and promoting the subsequent exchange reaction (~10-fold). In contrast to the mini-TAR annealing pathway, wherein NC-mediated annealing can initiate through both loop–loop kissing and a distinct "zipper" pathway involving nucleation at the 3′-/5′-terminal ends, full-length TAR hairpin annealing switches predominantly to the zipper pathway in the presence of saturated NC.

Keywords: nucleic acid chaperone activity; HIV-1 nucleocapsid protein; TAR RNA/DNA annealing; minus-strand transfer; nucleic acid aggregation

Introduction

HIV-1 (human immunodeficiency virus type 1) is a retrovirus that contains its genomic information in the form of two identical single-stranded RNA molecules. Conversion of the RNA genome into double-stranded viral DNA is an essential step of the retroviral life cycle. Reverse transcription involves multiple steps, including several nucleic acid (NA) rearrangements catalyzed by the HIV-1 nucleocapsid protein (NC). NC has been shown to facilitate annealing of the tRNA primer onto the primer binding site,[1–4] annealing of complementary RNA/DNA repeat regions in minus-strand transfer,[5–11] and annealing of complementary DNA sequences in plus-strand transfer.[7,12–14] HIV-1 NC is a short and basic NA binding protein that contains two zinc finger domains, each of which has an invariant CCHC metal-ion binding motif.[15–18] The mature

*Corresponding authors. E-mail addresses: rouzi002@umn.edu; musier@chemistry.ohio-state.edu.

Present address: M.-N. Vo, The Scripps Research Institute, 10550 North Torrey Pines Road, La Jolla, CA 92037, USA.

Abbreviations used: NC, nucleocapsid protein; TAR, transactivation response element; NA, nucleic acid; WT, wild type.

protein is produced by proteolytic cleavage of the Gag precursor and is found in the interior of the virus particle, where it is tightly associated with genomic RNA.[19]

NC has multiple functions during the viral replication cycle. In addition to playing an essential role in reverse transcription, NC or the NC domain of Gag has been shown to facilitate genomic RNA packaging, virus assembly, and integration.[20–24] Many of these functions rely on the NA chaperone activity of NC, which promotes NA rearrangements leading to thermodynamically more stable structures.[22–26] The chaperone function of NC relies on two main activities, NA aggregation[27–30] and duplex destabilization,[31–38] associated with the cationic N-terminal domain and zinc fingers, respectively.

It has recently been shown that synthesis of long products during reverse transcription *in vitro* is facilitated under conditions of NA aggregation.[39] In addition, DNA synthesis at low reverse transcriptase concentrations became more processive under aggregating conditions and strand displacement synthesis of the last 99 nt, resulting in production of the DNA flap, was shown to be more efficient. Sedimentation analysis and gel-shift annealing studies performed under the same solution conditions as a function of NC concentration showed that NA aggregation and annealing activities closely parallel each other.[30]

Annealing of the transactivation response element (TAR) DNA hairpin to a complementary TAR RNA hairpin, an essential step in minus-strand transfer, was shown to be accelerated by NC by as much as 3000-fold.[11] Previous studies used model 27-nt mini-TAR RNA and DNA hairpins derived from the top hairpin loop region of TAR to elucidate the mechanism of NC-mediated TAR RNA/DNA annealing.[30] This study shows that the complementary mini-TAR RNA and DNA hairpins anneal *via* a two-step pathway:

$$R + D \underset{k_{-1}}{\overset{k_1 D}{\rightleftharpoons}} RD^* \underset{k_{-2}}{\overset{k_2}{\rightleftharpoons}} RD \qquad (1)$$

Here, the first bimolecular step leads to the formation of the annealing intermediate *RD**, with the forward association rate constant k_1 and the intermediate dissociation rate k_{-1}. The annealing intermediate *RD** is subsequently converted into the fully annealed RNA/DNA duplex *RD via* a second monomolecular step that is characterized by the strand exchange rate k_2 and the reverse rate k_{-2}. DNA mutagenesis data showed that in the absence of NC, mini-TAR RNA/DNA annealing is nucleated *via* an extended loop–loop "kissing" interaction.[30] The annealing intermediate in this case involves 17 intermolecular base pairs, including nucleotides from the hairpin loop and from the adjacent stem and 3-nt bulge (Fig. 1). In the presence of saturating amounts of NC, an additional annealing pathway was observed, involving nucleation near the 3′/5′ ends.[30] The latter pathway has also been termed the "zipper" mechanism (Fig. 1).[41] Multiple annealing pathways have also been proposed for annealing of full-length TAR DNA to complementary DNA oligonucleotides based on single-molecule studies.[41] However, a kinetic analysis using full-length TAR RNA/DNA hairpins derived from the HIV-1 MAL isolate and NC(12–55) concluded that NC facilitated this annealing reaction primarily *via* the zipper pathway.[42] A recent single-molecule spectroscopy study using full-length TAR DNA/cDNA hairpins and full-length HIV-1 NC under nonaggregating conditions is consistent with this conclusion.[43]

In this work, we used gel-shift assays to systematically study the annealing kinetics of full-length 59-nt TAR RNA and DNA hairpins in the presence and in the absence of wild-type (WT) HIV-1 NC. The substrates and conditions used here were designed to closely mimic the *in vivo* process. In particular, use of full-length NC and gel-based rather than fluorescence-based assays allows reactions to be performed under conditions that promote NA aggregation. In addition, the role of RNA/DNA sequence complementarity and the NC concentration dependence of the annealing reaction were examined. The data obtained in the absence of NC support an overall slow two-step structure-based annealing mechanism, involving nucleation *via* a loop–loop kissing interaction followed by conversion to an extended annealed duplex. In contrast, the presence of saturating NC switches the annealing mechanism to the zipper pathway involving intermediate complex formation between the 3′/5′ ends of the hairpin stems.

Results and Discussion

As observed previously for mini-TAR RNA/DNA annealing,[30] under all conditions examined here, the annealing kinetics appears to be biexponential and the percentage of the molecules annealed as a function of time, $P(t)$, can be described by the fast and slow rates, k_f and k_s, respectively, and the fraction of the fast component f according to:

$$P(t) = P_\infty \cdot \left(f \cdot \left(1 - e^{-k_f t}\right) + (1 - f) \cdot \left(1 - e^{-k_s t}\right)\right). \qquad (2)$$

Previous studies[30] showed that k_f and k_s correspond to the rate of formation of the intermediate and that of the fully annealed duplex, respectively. The fraction of the fast component f is the probability of intermediate formation, and P_∞ is the final equilibrium percentage of RNA annealed. The following equations describe the relationship between these kinetic parameters and the elementary rates of the two-step process:[44]

$$k_f = k_1 D + k_{-1} \text{ and } k_s = f \cdot k_2 + k_{-2}, \qquad (3)$$

where

$$f = \frac{k_1 D}{k_1 D + k_{-1}} = \frac{D/K_d^*}{D/K_d^* + 1} \text{ and}$$
$$P_\infty = 100 \cdot f \cdot \frac{k_2}{k_2 + k_{-2}} = 100 \cdot \frac{D/K_d}{D/K_d + 1} \qquad (4)$$

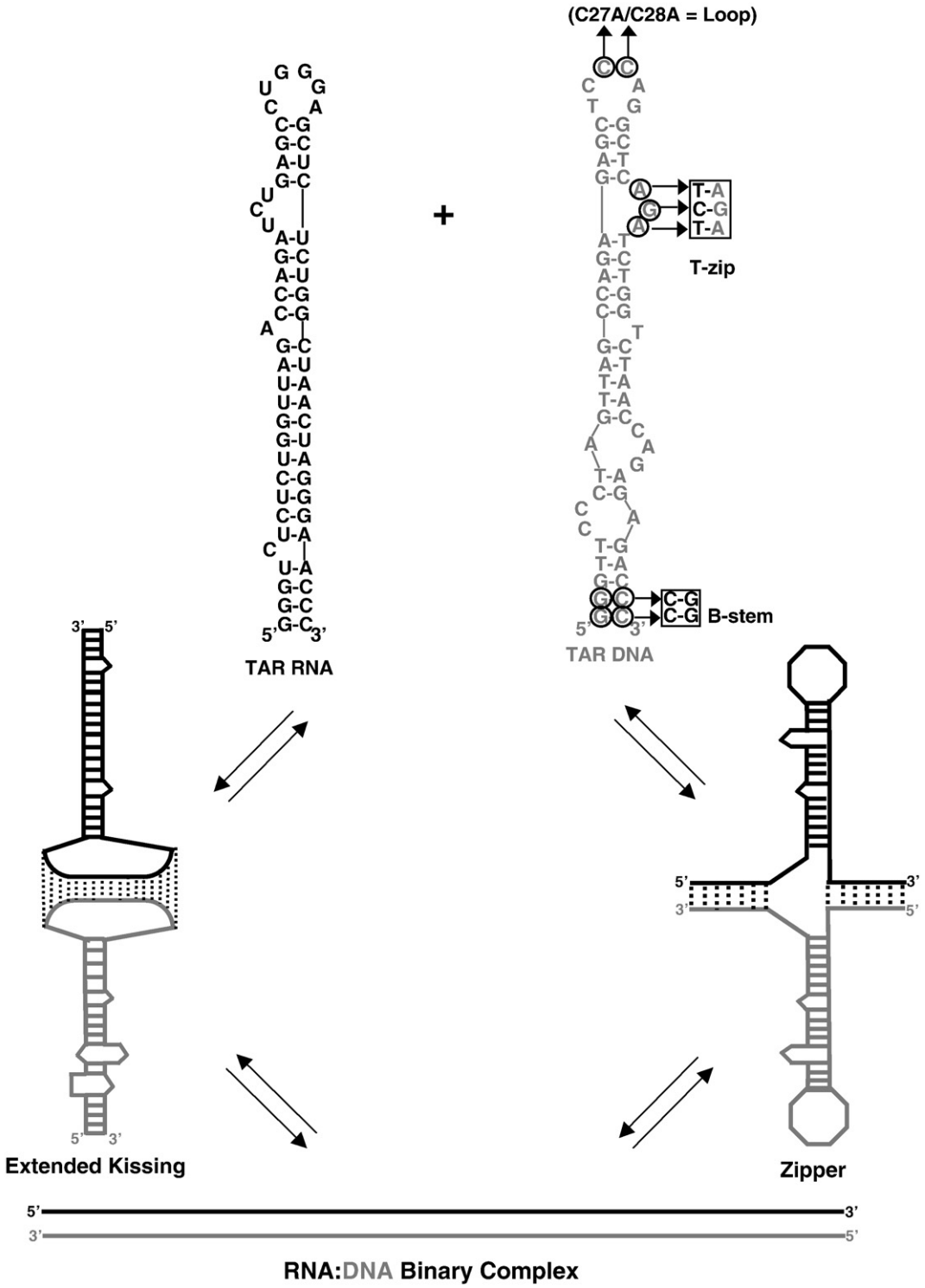

Fig. 1. Two pathways of full-length TAR RNA/DNA annealing. Top: predicted secondary structures of full-length TAR RNA (black) and TAR DNA (gray) hairpins. Sequences were derived from the HIV-1 NL4-3 isolate. The TAR RNA and DNA secondary structures were predicted by *m*-fold analysis.[40] Residues mutated in different DNA constructs are encircled. Bottom: (left) loop–loop "kissing" pathway, which involves initial formation of an extended kissing complex followed by subsequent strand exchange to form the fully annealed duplex, and (right) "zipper" pathway involving nucleation through the 3′/5′ termini resulting in formation of a zipper intermediate followed by conversion to the fully annealed duplex.

Here, K_d* and K_d are the equilibrium dissociation constants of the intermediate *RD** and the final annealed product *RD*, respectively. Experimentally, both rates are observed when they are sufficiently different from each other (i.e., $k_f \gg k_s$) and when the intermediate complex is reasonably stable (i.e.,

$0.1<f<1$). The annealing of the TAR molecules shown in Fig. 1 is strongly driven by formation of 14 new base pairs, such that the TAR hairpins anneal irreversibly both in the presence and in the absence of NC (i.e., $P_\infty = 100\%$) and k_{-2} is negligible. In addition, under all conditions examined here, the slow rate k_s is proportional to f, in accord with the second relationship in Eq. (3).

According to Eqs. (3) and (4), the fitted parameters k_f, k_s, and f can be used to estimate the elementary rates of the two-step annealing process using the following relationship:

$$k_1 = k_f \cdot \frac{f}{D},\ k_{-1} = k_f \cdot (1-f),\ k_2 = k_s/f,$$
$$K_d^* = \frac{k_{-1}}{k_1} = \frac{1-f}{f} \cdot D \qquad (5)$$

Kinetics of full-length TAR RNA/DNA annealing in the absence of NC

Dependence of full-length TAR RNA/DNA annealing kinetics on the concentration of TAR DNA

Figure 1 shows the full-length 59-nt TAR RNA and TAR DNA substrates used in this work. Gel-shift assays with [^{32}P]TAR RNA and unlabeled TAR DNA were used to quantitatively monitor complex formation as a function of time. Typical annealing time courses are shown in Fig. 2a. The annealing reactions were performed using several TAR DNA concentrations, with DNA in large excess over TAR RNA. In the absence of NC, the annealing reaction is extremely slow and irreversible. Under these pseudo-first-order conditions, the reaction rate increases with increasing DNA concentration, which is consistent with a bimolecular association. The annealing time courses in Fig. 2b were fit to the general two-exponential expression (Eq. (2)) to obtain k_s, k_f, and f in order to quantitatively analyze the annealing kinetics. P_∞ was set to 100% since the reaction is irreversible.

The fraction of the fast component, f, is very small (<0.1) but increases with increasing DNA concentration, D. The D dependence of the dominant slow annealing rate, k_s, is presented in the insert in Fig. 2b. As expected, k_s increases proportionally to D and the slope of k_s *versus* D yields an apparent bimolecular association rate constant, k_{eff}, of 10 ± 5 M^{-1} s^{-1}. The small probability of intermediate formation (i.e., $f \ll 1$) and the slow strand exchange rate both contribute to the extremely slow overall rate of annealing observed in the absence of NC. As shown in Fig. 2c, increasing temperature leads to a moderate rate enhancement. van't Hoff analysis of these data yields an enthalpy for the rate-limiting step of $\Delta H = 27\pm10$ kcal/mol (data not shown). This value is comparable with the ΔH value determined for mini-TAR annealing ($\Delta H = 15\pm5$ kcal/mol).[30] This result is consistent with the hypothesis that mini-TAR and TAR anneal *via* the same pathway in the absence of NC. Interestingly, TAR annealing is

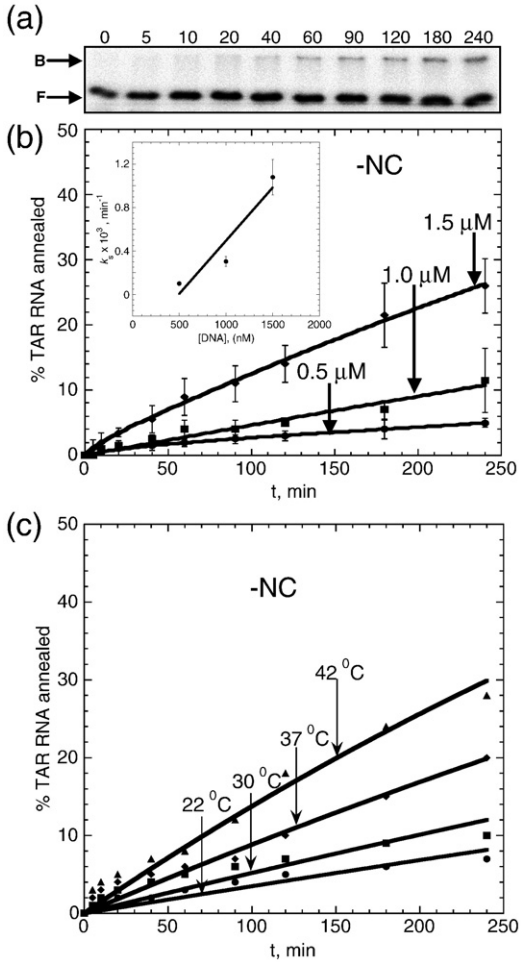

Fig. 2. Time course of TAR RNA/DNA hairpin annealing in the absence of NC. (a) Typical gel-shift analysis performed with 50 nM TAR RNA and 1 μM TAR DNA as a function of time. The numbers at the top of each lane correspond to minutes. Bound (B) and free (F) RNA bands are labeled on the left. (b) Time course showing the percentage of TAR RNA (15 nM) annealed to variable concentrations of TAR DNA (as indicated on each curve) at 37 °C. Lines represent double-exponential fits of the data to Eq. (2), with the equilibrium percentage annealed fixed at 100%. The inset shows the dominant slow annealing rate, k_s, obtained from the fits of the data shown in (b), as a function of TAR DNA concentration, D. The line is a linear fit of the data with a slope corresponding to $k_{eff} = 10\pm5$ M^{-1} s^{-1}. (c) Temperature dependence of TAR RNA/DNA annealing. Time courses for TAR RNA (15 nM) annealing to TAR DNA (1.5 μM) were measured in the absence of NC in 20 mM Na^+ at the indicated temperatures.

~10-fold slower than mini-TAR annealing in the absence of protein chaperone.[30] We hypothesize that this is due to the larger entropy loss upon intermediate complex formation in the case of the longer hairpins.[45] Alternatively, slower annealing of longer hairpins may be due to a greater electrostatic repulsion. However, an analysis of the salt dependence of the TAR annealing kinetics does not support the latter explanation.[46]

DNA mutational analysis

Kinetic studies were performed using various mutant TAR DNA hairpins to determine the pathway of full-length TAR RNA/DNA annealing. Assays were performed in the presence of 100 mM Mg^{2+}, which is known to facilitate the annealing reaction without altering the annealing pathway, to allow for more accurate quantification of extremely slow annealing kinetics observed in the absence of NC.[46] The importance of loop–loop complementarity was examined by studying the annealing of TAR RNA to a double (C27A/C28A) loop mutant DNA hairpin (Fig. 1, right). Indeed, the C27A/C28A loop mutant displayed dramatically slower annealing compared with WT DNA (Fig. 3). In contrast, when the two G:C base pairs at the bottom of the stem are inverted (B-stem mutant, Fig. 1), the rate of annealing is unaffected (Fig. 3). These results suggest that loop–loop complementarity is critical for full-length TAR RNA/DNA annealing, while stem-end complementarity is not. An additional TAR DNA variant was constructed containing a 3-nt insertion that results in closure of the 3-nt single-stranded bulge located near the top of the hairpin (T-zip, Fig. 1). This change creates 12 continuous base pairs adjacent to the hairpin loop and results in a dramatic reduction in the annealing rate (Fig. 3).

For all DNA mutants, the annealing kinetics measured in the presence of 100 mM Mg^{2+} was clearly biphasic. The k_f, k_s, and f parameters were determined by fitting the experimental annealing time courses shown in Fig. 3 to Eq. (2). The elementary reaction rates determined from these fits using Eq. (5) are plotted in Fig. 4. As shown in Fig. 4a, the intermediate association rate, k_1, decreased by ~7-fold when mutations were present in the top portion of the hairpin (i.e., Loop or T-zip). In contrast, the B-stem mutation had no effect on this rate. These results are consistent with a mechanism of TAR RNA/DNA annealing involving an extended loop–loop kissing intermediate (Fig. 1, lower left). As expected, based on this annealing pathway, the B-stem mutation does not affect k_1.

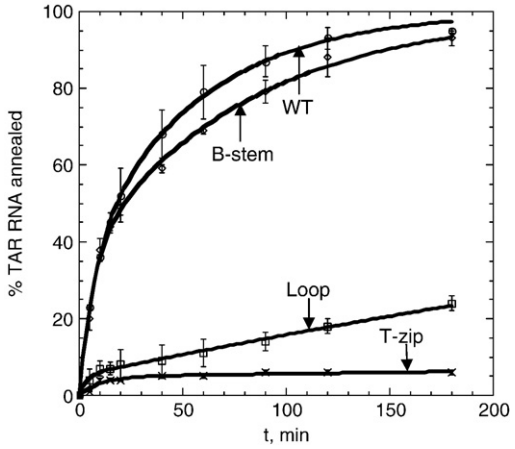

Fig. 3. Mutational analysis of TAR RNA/DNA annealing in the absence of NC. Percentage of TAR RNA (15 nM) annealed to various TAR DNA molecules (500 nM) as a function of time. The TAR DNA variants used are indicated by each curve (WT, Loop, T-zip, or B-stem, Fig. 1). Annealing was performed at 37 °C in the presence of 100 mM Mg^{2+}. Lines represent double-exponential fits of the data to Eq. (2), with the equilibrium percentage annealed fixed at 100%.

In agreement with these results, the intermediate dissociation rate, k_{-1}, was not significantly affected by T-zip or B-stem mutations but increased by ~5-fold in the presence of the Loop mutation (Fig. 4c). As a result of these changes in the "on" and "off" rates for the formation of the reaction intermediate, the intermediate dissociation constant, K_d^*, increased by ~30-fold and ~10-fold in the presence of Loop and T-zip mutations, respectively (Fig. 4b). Interestingly, the conversion rates, k_2 values, are similar (i.e., within 2-fold of WT) for all the TAR DNA constructs (Fig. 4d). The small value of this rate, $k_2 = 0.03 \pm 0.02$ min^{-1}, suggests that strand exchange is rate limited by the cooperative melting of a large portion of one or both stems, followed by much faster strand exchange. This hypothesis is consistent with the observation that k_2 is essentially the same for mini-TAR and TAR hairpins[46] (i.e., that the strand exchange rate does not depend on hairpin stem length). Taken together, these data are consistent with an annealing mechanism in the absence of NC that involves nucleation through an extended loop–loop kissing interaction followed by slower conversion to a fully extended annealed duplex.

Kinetics of full-length TAR RNA/DNA annealing in the presence of NC

NC greatly facilitates full-length TAR RNA/DNA annealing. The time course of annealing in the presence of saturating amounts of NC (4:1 nt/NC ratio in low salt buffer; i.e., 20 mM Na^+ and 0.2 mM Mg^{2+}) is well described by a single-exponential expression (Fig. 5). The final yield of annealed product in the reactions shown in Fig. 5b (D = 30–90 nM) is close to 100%. Fitting the annealing time courses to a single-exponential expression yields an annealing rate of 4 ± 2 min^{-1}. Although the annealing rate appears to be independent of D under these conditions (due to the time resolution of the assay), experiments performed at lower D (10–20 nM) show a reduced rate consistent with a bimolecular annealing mechanism (inset in Fig. 5b). The equilibrium percentage of annealed product also decreases at lower D, suggesting that the annealing reaction is reversible under these conditions, as observed previously.[30] The annealing rate measured for D = 30–60 nM is ~10-fold faster than the rate of NC-facilitated mini-TAR RNA/DNA annealing at a similar D.[30] Given that TAR anneals ~10-fold slower in the absence of NC, the overall NC-facilitated rate enhancement is ~100-fold greater for full-length TAR annealing compared with mini-TAR.

Increasing temperature facilitates TAR annealing further (Fig. 5c). The van't Hoff analysis of the temperature dependence of the dominant fast rate

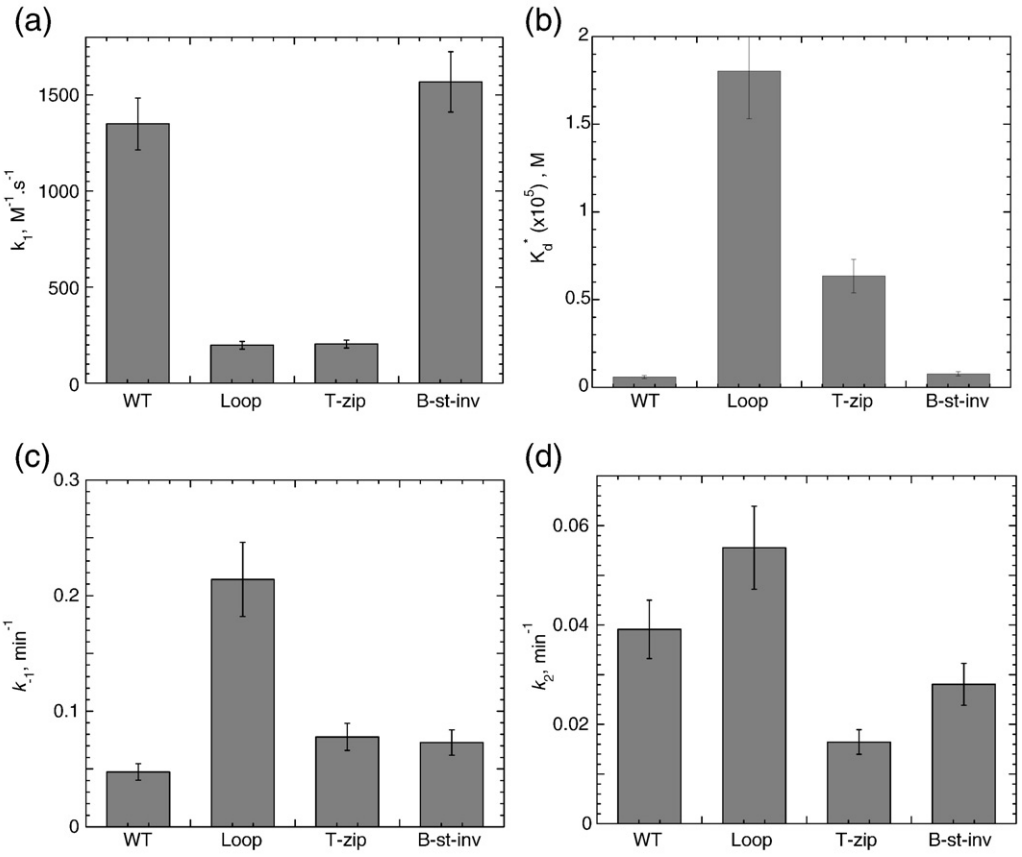

Fig. 4. Elementary reaction rates and intermediate dissociation constant for annealing of TAR RNA to various TAR DNA constructs in the absence of NC. The elementary rates [(a) k_1; (c) k_{-1}; (d) k_2] and intermediate dissociation constant (b) for the two-step annealing process were obtained by analysis of annealing time courses in Fig. 3 using Eqs. (2)–(5).

(data not shown) yields an enthalpy for the rate-limiting step of 28±8 kcal/mol, consistent with extensive melting occurring prior to complex formation. This enthalpy value is ~2-fold higher than that previously reported for mini-TAR annealing.[30] This result implies that in the presence of saturating amounts of NC, annealing of longer TAR hairpins involves premelting of the more stable region compared with the case of mini-TAR hairpin annealing.

DNA mutational analysis

We next used the mutant TAR DNA constructs shown in Fig. 1 (right) to investigate the annealing pathway of full-length TAR in the presence of saturating amounts of NC. Under these conditions, annealing in the presence of the Loop or T-zip variant is very fast and similar to that of the WT DNA (Fig. 6). In contrast, the annealing rate with the B-stem variant is significantly reduced. The fast component dominates annealing (i.e., f of ~1), thus making determination of k_{-1} and k_2 rates less reliable than that in the absence of NC. The effects of TAR DNA mutations on the elementary annealing rates are summarized in Fig. 7. Relative to the reactions performed in the absence of NC, saturating amounts of NC resulted in 100-fold faster k_1 for WT, Loop, and T-zip mutant TAR DNA. In contrast, k_1 was ~6-fold slower for the B-stem mutant (Fig. 7a). The intermediate complex dissociation rates, k_{-1} values, were similar for all the TAR DNA constructs, with slightly faster dissociation measured for the B-stem variant (Fig. 7c). In part as a result of this but largely due to the differences in k_1, the reaction intermediate was 1 order of magnitude more stable for the WT, Loop, and T-zip TAR constructs relative to the B-stem variant (Fig. 7b). These results are consistent with an annealing pathway that involves nucleation *via* the stem ends. The B-stem mutation introduces noncomplementarity between DNA and RNA in this region, thereby making intermediate association slower and dissociation faster at this nucleation site. The strand exchange rates, k_2 values, are similar for WT, Loop mutant, and B-stem mutant. The ~10-fold slower exchange rate determined for the T-zip mutant may be due to stabilization of the stem by introduction of three additional base pairs (Fig. 7d). Taken together, these data are consistent with WT TAR RNA/DNA annealing *via* the zipper pathway in the presence of saturating amounts of NC.

Effect of varying NC concentration on WT and mutant TAR DNA annealing

The annealing of 15 nM TAR RNA to 150 nM WT or mutant TAR DNA was measured in the presence

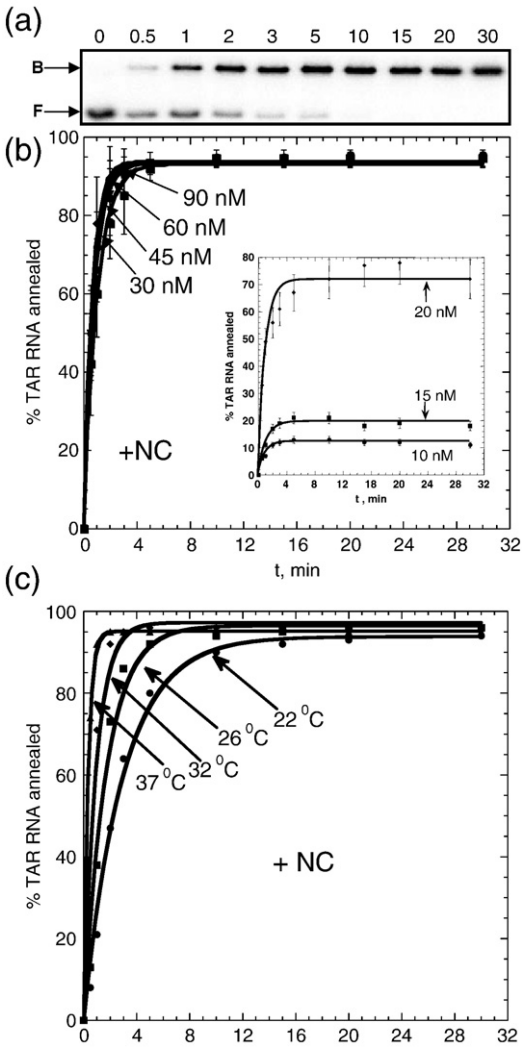

Fig. 5. Time course of TAR RNA/DNA hairpin annealing in the presence of saturating amounts of NC. (a) Typical gel-shift analysis performed with 15 nM TAR RNA and 45 nM TAR DNA. The numbers at the top of each lane correspond to minutes. The positions of bound (B) and free (F) RNA bands are indicated on the left. (b) Time dependence of the percentage of TAR RNA (15 nM) annealed to variable concentrations of TAR DNA (as indicated by each curve) at 37 °C and a 4:1 nt/NC ratio. The 10–20 nM DNA curves are shown as an inset. (c) TAR RNA/DNA annealing time courses (15 nM TAR RNA + 45 nM TAR DNA) obtained at different temperatures, as indicated in the figure. All lines are single-exponential fits of the data.

of varying concentrations of NC to examine the NC-induced TAR RNA/DNA annealing pathway switch in more detail (Fig. 8). The latter is presented as fractional NA saturation with NC, Θ_{NC}. Under these low salt conditions (20 mM Na^+ and 0.2 mM Mg^{2+}), all added NC is bound to NA and Θ_{NC} can be calculated as

$$\Theta_{NC} = (NC : nt) \times 6, \quad (6)$$

where NC:nt is the protein-to-nucleotide concentration ratio and assuming that 1 NC binds to 6±1 nucleotides at saturation.[11,22–24,36,47–50] As expected, at saturation (i.e., $\Theta_{NC} \geq 1$), annealing in the presence of the Loop mutant DNA (Fig. 8b) is very fast and similar to that of WT (Fig. 8a), whereas annealing with the B-stem variant is slightly suppressed (Fig. 8c). Further decrease in Θ_{NC} ($\Theta_{NC} = 0.75$) leads to a significant reduction of the annealing rate for both B-stem and Loop mutants compared with WT DNA, with a more pronounced effect on the latter. These results suggest that under slightly subsaturating concentrations of NC, full-length TAR RNA/DNA annealing occurs with comparable efficiency *via* both kissing and zipper pathways, with annealing *via* the stem ends slightly favored. This is consistent with the preferential annealing of WT TAR RNA/DNA *via* the zipper pathway under saturated NC binding conditions.

The dissociation constant for the annealing intermediate and the elementary rates for the two-step reaction, determined based on the data shown in Fig. 8, are presented in Fig. 9. The elementary rates could only be determined for $\Theta_{NC} \geq 0.375$ since the annealing is extremely slow and has a negligible fast component at lower Θ_{NC}. In addition, k_2 cannot be determined at $\Theta_{NC} > 0.75$ since the annealing is dominated by the fast component. Figure 9a shows that the B-stem mutant has the slowest association rates over the range of $0.375 \leq \Theta_{NC} \leq 1.5$. The Loop mutant has a slightly faster k_1 than the B-stem mutant but remains slower than the WT. While k_1 is very fast for all the TAR DNA constructs tested at high Θ_{NC}, WT TAR DNA requires less NC to reach its maximum k_1. These results are consistent with the existence of multiple annealing pathways, with a greater contribution from the zipper pathway when $\Theta_{NC} \geq 0.4$.

There is no significant difference in the intermediate dissociation rate, k_{-1}, between WT TAR DNA and the two mutant constructs (Fig. 9c), suggesting

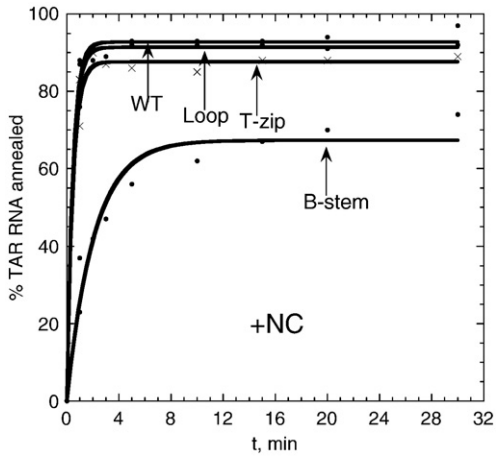

Fig. 6. Mutational analysis of full-length TAR RNA/DNA annealing in the presence of saturating amounts of NC. Percentage of TAR RNA (15 nM) annealed to various TAR DNA constructs (45 nM), as indicated on each curve (WT, Loop, T-zip, or B-stem, Fig. 1), as a function of time at 37 °C in the presence of a 4:1 nt/NC ratio. Lines represent single-exponential fits of the data.

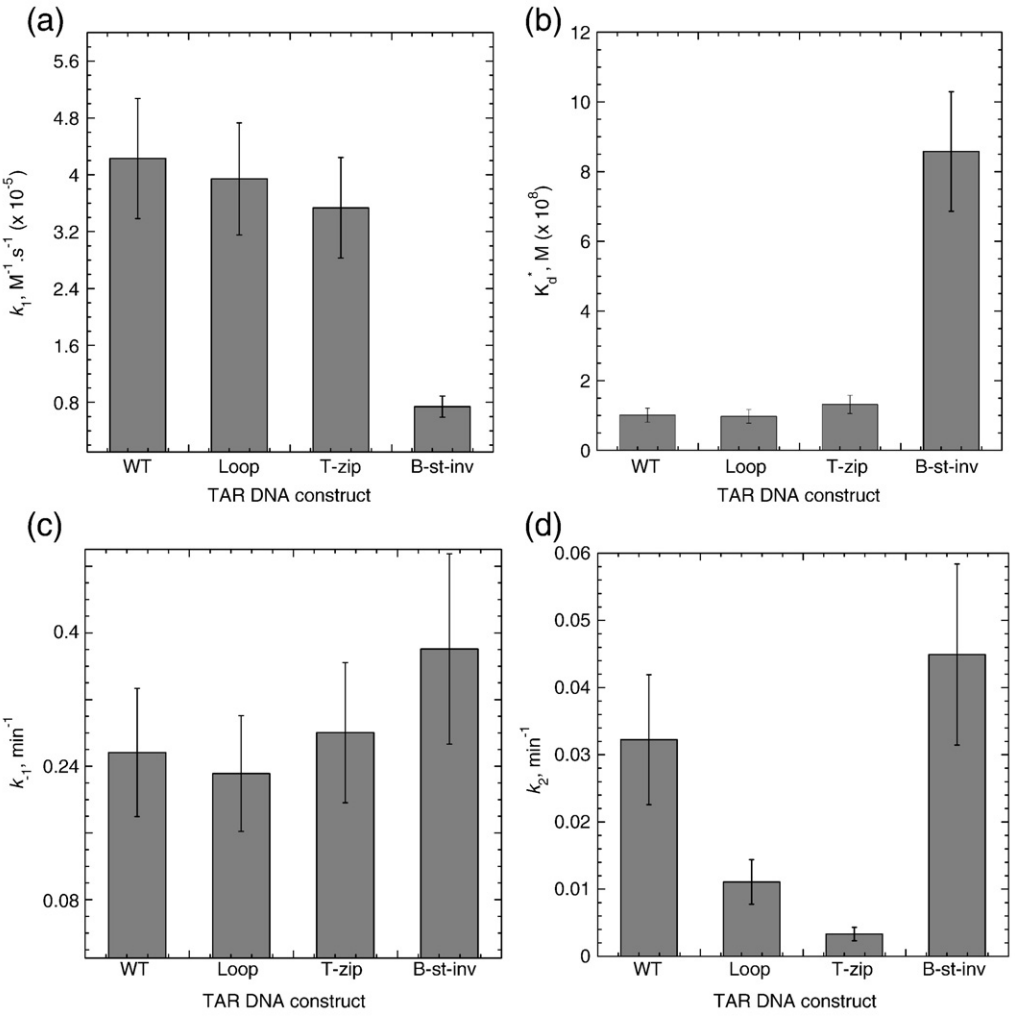

Fig. 7. Comparison of elementary rates and intermediate dissociation constant of WT and mutant TAR DNA constructs in the presence of saturating concentrations of NC. Elementary rates [(a) k_1; (c) k_{-1}; (d) k_2] and intermediate dissociation constants (b) were obtained by using Eqs. (2)–(5) to analyze the annealing time courses presented in Fig. 6 for TAR RNA (15 nM) annealed to various TAR DNA constructs (45 nM) at 37 °C and a 4:1 nt/NC ratio.

that dissociation of the intermediate formed with either the Loop or B-stem variant is comparable in the range of Θ_{NC} studied here. The same conclusion holds for k_2, which also appears to be independent of Θ_{NC} (Fig. 9d). Based on the known duplex-destabilizing ability of NC, one would expect k_2 to increase with increasing NC concentration. However, we hypothesize that this dependence is most likely obscured by the NC-induced annealing pathway switch from the extended loop–loop kissing pathway to the zipper pathway at the Θ_{NC} of ~0.4. This switch is not abrupt; both pathways contribute to annealing, with the zipper contribution taking over completely upon NC saturation.

Role of NC-induced NA aggregation

The major effect of increasing NC concentration is enhancement of the bimolecular association step of annealing (Fig. 9a). This, in turn, results in strong stabilization of the annealing intermediate (Fig. 9b). A sedimentation assay was performed to measure the fraction of aggregated full-length TAR RNA molecules, f_a, as a function of fractional NC binding under conditions similar to those for the annealing assays to examine the role of NC-induced NA aggregation in bimolecular intermediate stabilization. Figure 10 shows that the amount of NC required to stabilize the reaction intermediate [continuous line, $f(\Theta_{NC})$] is virtually equivalent to the amount needed to induce NA aggregation [dotted line, $f_a(\Theta_{NC})$]. These data are consistent with the results obtained for mini-TAR[30] and provide further support for the notion that NC-induced NA aggregation constitutes a major component of NC's chaperone function.

Summary and Conclusions

In this work, the mechanism of 59-nt TAR RNA/DNA hairpin annealing was examined as a function of NA saturation with HIV-1 NC. Under all solution conditions tested, TAR hairpins anneal *via*

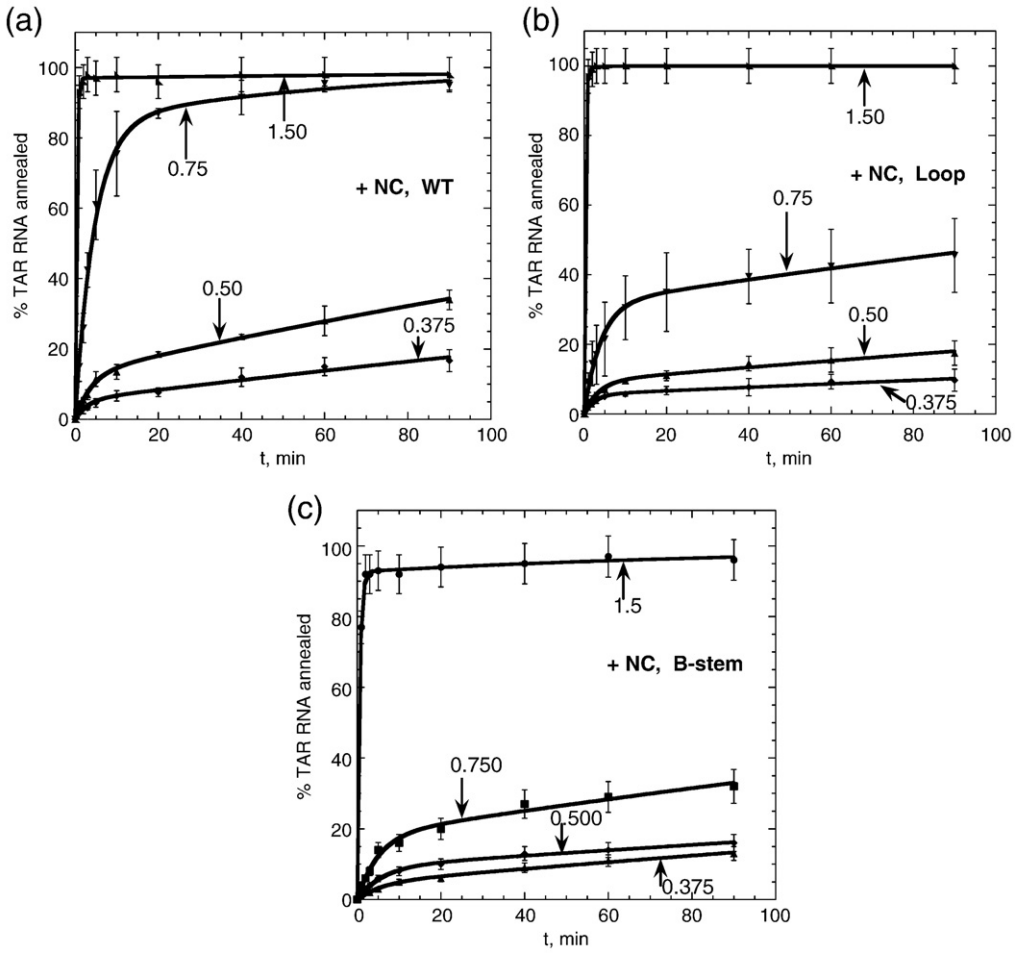

Fig. 8. Annealing of WT and mutant TAR DNA to TAR RNA in the presence of variable amounts of NC. TAR RNA (15 nM) was annealed to 150 nM of WT TAR DNA (a), Loop mutant TAR DNA (b), or B-stem mutant TAR DNA (c) as a function of time in the presence of various concentrations of NC in low salt (20 mM Na^+, 0.2 mM Mg^{2+}). Fractional NA saturation with NC, Θ_{NC}, calculated according to Eq. (6), is indicated for each curve. Lines represent double-exponential fits of the data.

the two-step pathway described by Eq. (1), involving formation of a bimolecular annealing intermediate in preequilibrium with the subsequent strand exchange step resulting in the fully annealed RNA/DNA duplex. Interestingly, the nature of the annealing intermediate (i.e., the annealing pathway) changes as more NC is added. DNA mutational analysis showed that in the absence of NC or at low NC binding levels, TAR RNA/DNA annealing proceeds *via* an extended loop–loop kissing intermediate (Fig. 1, lower left). In contrast, when levels of NC binding approach saturation, TAR RNA/DNA anneals through the stem ends (Fig. 1, lower right). Both pathways contribute to annealing at intermediate levels of NC binding (Fig. 9a and b).

We hypothesize that the existence of two competing pathways for annealing of the TAR RNA/DNA hairpins is due to the comparable stabilities of the two 4-bp helical segments in TAR RNA (Fig. 1, top left). In particular, based on theoretical predictions, the 4-bp helix adjacent to the hairpin loop is ~1 kcal/mol more stable than the 4-bp helix proximal to the 5′/3′ termini.[40,51] While melting of the more stable helix is less probable, it allows for formation of a 17-bp extended loop–loop intermediate (Fig. 1, lower left). In contrast, melting of the terminal 4-bp helix leads to the formation of an RNA/DNA intermediate containing only 9 bp. Whereas the former pathway is plausible in the absence of NC, in the presence of saturated NC, which stabilizes both intermediates, the annealing switches to the pathway that requires the least structure premelting (i.e., the zipper pathway).

Previous studies on the annealing of mini-TAR RNA/DNA were also consistent with two annealing pathways, with the loop pathway dominating in the absence of NC.[30] However, in the case of the shorter hairpin, which only contains two helical regions of similar stability, the stem pathway does not dominate even at saturated NC.[30]

A recent study examined the annealing of small complementary DNA hairpins, PBS(+) and PBS(−), representing the rate-limiting step of plus-strand transfer during reverse transcription.[52] A truncated version of NC, NC(12–55), which lacks the N-terminal basic domain and is therefore a poor aggre-

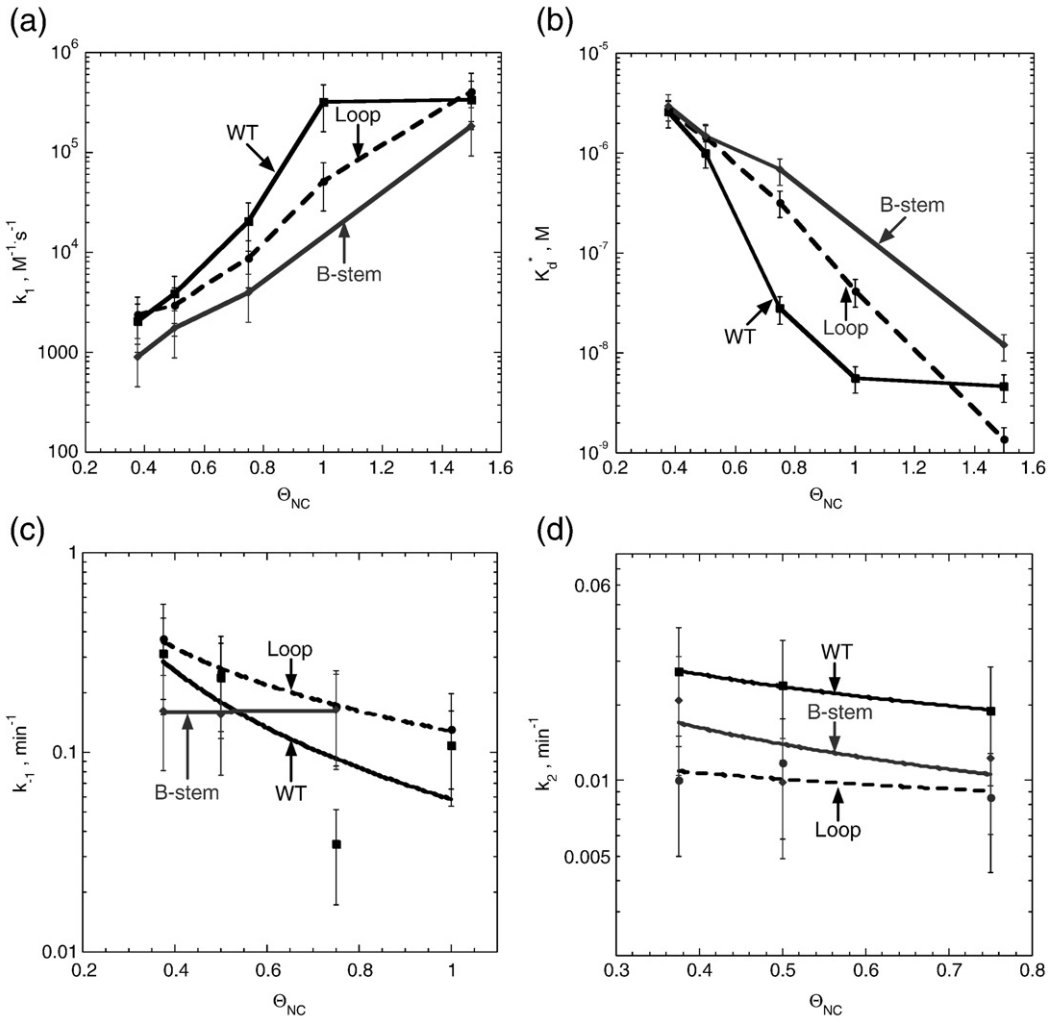

Fig. 9. Comparison of elementary rates [(a), (c), and (d)] and intermediate dissociation constants (b) for annealing of WT and mutant TAR DNA hairpins to TAR RNA in the presence of variable amounts of NC. Fractional NA saturation with NC, Θ_{NC}, was calculated according to Eq. (6). Parameters were obtained using Eqs. (2)–(5) for the analysis of the annealing time courses presented in Fig. 8.

gating agent, was also able to induce a pathway switch as compared with the reaction performed in the absence of NC.[52] Another study from the same group examined the effect of NC(12–55) on the annealing of TAR DNA to its DNA complement cTAR.[42] As in the PBS annealing study,[52] NC(12–55) stimulated the TAR annealing reaction by ~100-fold. This is lower than the ~10^3-fold and ~10^5-fold stimulations observed for mini-TAR[30] and TAR annealing (this work), respectively, using full-length NC(1–55). Indeed, we have shown that the duplex-destabilizing and minor aggregation activities of NC(12–55) each contributes ~10-fold to the overall rate enhancement (M.-N. Vo, M. Mitra, I. Rouzina, and K. Musier-Forsyth, unpublished results). Taken together, these results support a major role for NC-induced NA aggregation in its chaperone activity.

NC modulates the annealing pathway of structured complementary NA *via* both of its major activities, NA aggregation and destabilization.[4,26,30] *In vivo*, these diverse capabilities of NC may ensure efficient obligatory and random strand transfer events during reverse transcription.[53,54] The major effect of NC on the efficiency of strand transfers may also explain the increased production of full-length RNA transcripts during *in vitro* reverse transcription,[39] as well as improved strand displacement synthesis of the central DNA flap[55] and greater reverse transcriptase processivity,[55] which are both observed under conditions that also promote NC-induced NA aggregation.[39,55]

Materials and Methods

Protein, RNA, and DNA preparation

The NC used in this work was prepared by solid-phase synthesis as described previously,[41] and its purity was estimated to be >95% by SDS-PAGE. The concentration of NC was determined by measuring its absorbance at 280 nm and using $\varepsilon_{280} = 6050\ mol^{-1}\ cm^{-1}$.

All DNA oligonucleotides were purchased from Integrated DNA Technologies (Coralville, IA). Full-length

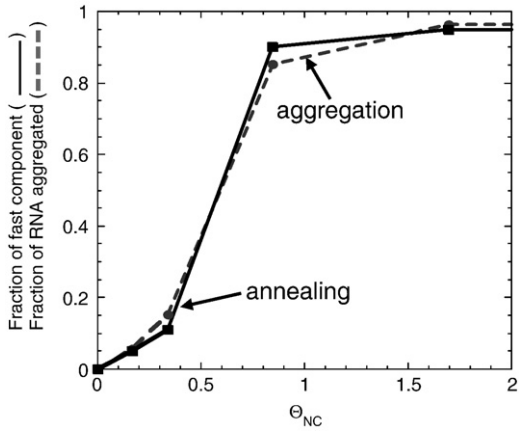

Fig. 10. Fraction of the fast annealing component (f) and aggregated fraction of TAR RNA (f_a) as a function of fractional NA saturation with NC. f was obtained from the analysis of the data presented in Fig. 8 using Eqs. (2)–(5). f_a was obtained by sedimentation assays as described in Materials and Methods, carried out under the same solution conditions as for the annealing experiments.

TAR RNA was generated by *in vitro* transcription using a PCR-amplified template encoding the 59-nt TAR sequence downstream of a T7 RNA polymerase promoter. The T7 promoter was appended during the PCR; the sequences of DNA template and primers for the PCR were as follows: TAR DNA template, 5′-GGGTCTCT-CTGGTTAGACCAGATCTGAGCCTGGGAGCTCTC-TGGCTAACTAGGGAACCC-3′ with its complementary sequence 5′-GGGTTCCCTAGTTAGCCAGAGAGCTCC-CAGGCTCAGATCTGGTCTAACCAGAGAGACCC-3′; T7-TAR primer 1, 5′-CTGTAATACGACTCACTA-TAGGGTCTCTCTGGTTAGACCAG-3′; and TAR primer 2, 5′-GGGTTCCCTAGTTAGCCAGAGAGC-3′. PCRs were performed with *PfuTurbo* DNA polymerase (Stratagene, La Jolla, CA) according to the enzyme manufacturer's protocol using the provided buffer. Briefly, each reaction included 30 cycles of denaturation, annealing, and extension at temperatures of 94 °C for 45 s, 50 °C for 45 s, and 72 °C for 2 min, respectively, followed by 1 cycle of extension at 72 °C for 10 min. PCR-generated DNA template was extracted with phenol/chloroform/isoamyl alcohol (25:24:1, by volume) and precipitated with ethanol prior to use. The purified DNA template (5 μg per 100 μL of reaction) was *in vitro* transcribed according to standard procedures, followed by DNase treatment to remove the DNA template. All RNA and DNA oligonucleotides were gel purified on 12% (w/v) denaturing polyacrylamide gels, dissolved in diethyl pyrocarbonate-treated water, and stored at −20 °C. Full-length TAR RNA was internally ^{32}P labeled *via in vitro* transcription under similar conditions, except that the GTP concentration was lowered from 4 to 1 mM and 17 mCi/mL [α-^{32}P]GTP was added to the reaction.

The concentrations of the RNA and DNA oligonucleotides were determined by measuring their absorbances at 260 nm and using the following extinction coefficients: TAR RNA (59-mer), 5.34×10^5 M^{-1} cm^{-1}; TAR DNA (59-mer), 5.65×10^5 M^{-1} cm^{-1}; C27A/C28A TAR DNA (59-mer), 5.74×10^5 M^{-1} cm^{-1}; B-stem TAR DNA (59-mer), 5.65×10^5 M^{-1} cm^{-1}; and T-zip TAR DNA (62-mer), 5.80×10^5 M^{-1} cm^{-1}.

Prior to use, all oligonucleotides were refolded in 25 mM Hepes, pH 7.5, and 100 mM NaCl at a concentration 100× greater than that used in the annealing reactions. This was accomplished by incubation at 80 °C for 2 min and cooling to 60 °C for 2 min, followed by addition of $MgCl_2$ to a final concentration of 10 mM and placement on ice.

Annealing assays

For annealing assays, refolded ^{32}P-labeled full-length TAR RNA was combined with refolded unlabeled complementary WT or mutant TAR DNA constructs in a solution containing 20 mM Hepes, pH 7.5, 20 mM NaCl, and 0.2 mM $MgCl_2$ (this $MgCl_2$ concentration comes from the refolding buffer) at 37 °C, except when otherwise indicated.

In the absence of NC, DNA concentration dependence studies were performed with 50 nM RNA and various concentrations of DNA, as indicated in the figure legends. Reactions were initiated by adding DNA to RNA, followed by incubation in the reaction buffer for the indicated times. Reactions were quenched by placing solutions on ice, followed by addition of glycerol to 5% final concentration. Samples were loaded onto 12% SDS polyacrylamide gels [375 mM Tris–HCl, pH 8.8, 0.1% SDS, and 19:1 acrylamide/bisacrylamide (w/v)] run at 25 °C in Tris–glycine (25 mM Tris and 250 mM glycine, pH 8.3) running buffer.

In the presence of NC, studies on the DNA concentration dependence of TAR RNA/DNA annealing were performed by mixing 15 nM RNA with various concentrations of DNA prior to the addition of NC to achieve a 4:1 nucleotide/NC ratio. Thus, final NC concentrations were 0.664, 0.885, 1.11, and 1.55 μM in the presence of 30, 45, 60, and 90 nM TAR DNA, respectively. Annealing reactions were quenched at the indicated times by incubation with 1% (w/v) SDS and immediate placement on ice for 5 min. Samples were subjected to phenol/chloroform extraction (2×), followed by addition of glycerol to 5% final concentration and separation on 12% SDS-polyacrylamide gels as described earlier. Gels were visualized using a Bio-Rad Molecular Imager FX and quantified with Bio-Rad Quantity One software. NC concentration dependence studies were carried out similarly with 15 nM RNA and 150 nM DNA in the presence of various concentrations of NC, as indicated in the figure legends.

Sedimentation/aggregation assays

Refolded ^{32}P-labeled full-length TAR RNA (15 nM) was combined with TAR DNA (45 nM) in a solution containing 20 mM Hepes, pH 7.5, 20 mM NaCl, and 0.2 mM $MgCl_2$. Upon addition of NC to a final concentration of 0.1, 0.2, 0.5, 1.0, or 2.0 μM, reactions (40 μL) were incubated at 37 °C for 30 min. At the end of the incubation period, solutions were centrifuged at 12,000 rpm in a microcentrifuge for 20 min. Supernatant (5 μL) was collected and analyzed by scintillation counting. The percentage of radioactivity remaining in the supernatant relative to the RNA-only sample (set to 100%) was plotted as a function of NC concentration.

Acknowledgements

This research was supported by the National Institutes of Health through grant GM065056 (to

K.M.-F.) and predoctoral training grant T32 GM008700 (to M.-N.V). We thank Dr. Robert Gorelick (National Cancer Institute at Frederick) for NC purification and Drs. Daniel G. Mullen and Brandie Kovaleski (University of Minnesota) for chemical synthesis of NC.

References

1. Chan, B., Weidemaier, K., Yip, W. T., Barbara, P. F. & Musier-Forsyth, K. (1999). Intra-tRNA distance measurements for nucleocapsid protein-dependent tRNA unwinding during priming of HIV reverse transcription. *Proc. Natl Acad. Sci. USA*, **96**, 459–464.
2. De Rocquigny, H., Gabus, C., Vincent, A., Fournie-Zaluski, M. C., Roques, B. & Darlix, J. L. (1992). Viral RNA annealing activities of human immunodeficiency virus type 1 nucleocapsid protein require only peptide domains outside the zinc fingers. *Proc. Natl Acad. Sci. USA*, **89**, 6472–6476.
3. Feng, Y. X., Campbell, S., Harvin, D., Ehresmann, B., Ehresmann, C. & Rein, A. (1999). The human immunodeficiency virus type 1 Gag polyprotein has nucleic acid chaperone activity: possible role in dimerization of genomic RNA and placement of tRNA on the primer binding site. *J. Virol.* **73**, 4251–4256.
4. Hargittai, M. R., Gorelick, R. J., Rouzina, I. & Musier-Forsyth, K. (2004). Mechanistic insights into the kinetics of HIV-1 nucleocapsid protein-facilitated tRNA annealing to the primer binding site. *J. Mol. Biol.* **337**, 951–968.
5. Davis, W. R., Gabbara, S., Hupe, D. & Peliska, J. A. (1998). Actinomycin D inhibition of DNA strand transfer reactions catalyzed by HIV-1 reverse transcriptase and nucleocapsid protein. *Biochemistry*, **37**, 14213–14221.
6. Golinelli, M. P. & Hughes, S. H. (2003). Secondary structure in the nucleic acid affects the rate of HIV-1 nucleocapsid-mediated strand annealing. *Biochemistry*, **42**, 8153–8162.
7. Guo, J., Wu, T., Anderson, J., Kane, B. F., Johnson, D. G., Gorelick, R. J. *et al.* (2000). Zinc finger structures in the human immunodeficiency virus type 1 nucleocapsid protein facilitate efficient minus- and plus-strand transfer. *J. Virol.* **74**, 8980–8988.
8. Guo, J., Wu, T., Kane, B. F., Johnson, D. G., Henderson, L. E., Gorelick, R. J. & Levin, J. G. (2002). Subtle alterations of the native zinc finger structures have dramatic effects on the nucleic acid chaperone activity of human immunodeficiency virus type 1 nucleocapsid protein. *J. Virol.* **76**, 4370–4378.
9. Hong, M. K., Harbron, E. J., O'Connor, D. B., Guo, J., Barbara, P. F., Levin, J. G. & Musier-Forsyth, K. (2003). Nucleic acid conformational changes essential for HIV-1 nucleocapsid protein-mediated inhibition of self-priming in minus-strand transfer. *J. Mol. Biol.* **325**, 1–10.
10. Lapadat-Tapolsky, M., Pernelle, C., Borie, C. & Darlix, J. L. (1995). Analysis of the nucleic acid annealing activities of nucleocapsid protein from HIV-1. *Nucleic Acids Res.* **23**, 2434–2441.
11. You, J. C. & McHenry, C. S. (1994). Human immunodeficiency virus nucleocapsid protein accelerates strand transfer of the terminally redundant sequences involved in reverse transcription. *J. Biol. Chem.* **269**, 31491–31495.
12. Johnson, P. E., Turner, R. B., Wu, Z. R., Hairston, L., Guo, J., Levin, J. G. & Summers, M. F. (2000). A mechanism for plus-strand transfer enhancement by the HIV-1 nucleocapsid protein during reverse transcription. *Biochemistry*, **39**, 9084–9091.
13. Muthuswami, R., Chen, J., Burnett, B. P., Thimmig, R. L., Janjic, N. & McHenry, C. S. (2002). The HIV plus-strand transfer reaction: determination of replication-competent intermediates and identification of a novel lentiviral element, the primer over-extension sequence. *J. Mol. Biol.* **315**, 311–323.
14. Wu, T., Guo, J., Bess, J., Henderson, L. E. & Levin, J. G. (1999). Molecular requirements for human immunodeficiency virus type 1 plus-strand transfer: analysis in reconstituted and endogenous reverse transcription systems. *J. Virol.* **73**, 4794–4805.
15. Berg, J. M. (1986). Potential metal-binding domains in nucleic acid binding proteins. *Science*, **232**, 485–487.
16. Covey, S. N. (1986). Amino acid sequence homology in gag region of reverse transcribing elements and the coat protein gene of cauliflower mosaic virus. *Nucleic Acids Res.* **14**, 623–633.
17. Green, L. M. & Berg, J. M. (1990). Retroviral nucleocapsid protein–metal ion interactions: folding and sequence variants. *Proc. Natl Acad. Sci. USA*, **87**, 6403–6407.
18. Henderson, L. E., Copeland, T. D., Sowder, R. C., Smythers, G. W. & Oroszlan, S. (1981). Primary structure of the low molecular weight nucleic acid-binding proteins of murine leukemia viruses. *J. Biol. Chem.* **256**, 8400–8406.
19. Coffin, J. M., Hughes, S. H. & Varmus, H. E. (1997). *Retroviruses.* Cold Spring Harbor Laboratory Press, Cold Spring Harbor, NY.
20. Carteau, S., Gorelick, R. J. & Bushman, F. D. (1999). Coupled integration of human immunodeficiency virus type 1 cDNA ends by purified integrase *in vitro*: stimulation by the viral nucleocapsid protein. *J. Virol.* **73**, 6670–6679.
21. Cristofari, G. & Darlix, J. L. (2002). The ubiquitous nature of RNA chaperone proteins. *Prog. Nucleic Acid Res. Mol. Biol.* **72**, 223–268.
22. Darlix, J. L., Lapadat-Tapolsky, M., de Rocquigny, H. & Roques, B. P. (1995). First glimpses at structure–function relationships of the nucleocapsid protein of retroviruses. *J. Mol. Biol.* **254**, 523–537.
23. Rein, A., Henderson, L. E. & Levin, J. G. (1998). Nucleic-acid-chaperone activity of retroviral nucleocapsid proteins: significance for viral replication. *Trends Biochem. Sci.* **23**, 297–301.
24. Tsuchihashi, Z. & Brown, P. O. (1994). DNA strand exchange and selective DNA annealing promoted by the human immunodeficiency virus type 1 nucleocapsid protein. *J. Virol.* **68**, 5863–5870.
25. Bampi, C., Jacquenet, S., Lener, D., Decimo, D. & Darlix, J. L. (2004). The chaperoning and assistance roles of the HIV-1 nucleocapsid protein in proviral DNA synthesis and maintenance. *Curr. HIV Res.* **2**, 79–92.
26. Levin, J. G., Guo, J., Rouzina, I. & Musier-Forsyth, K. (2005). Nucleic acid chaperone activity of HIV-1 nucleocapsid protein: critical role in reverse transcription and molecular mechanism. *Prog. Nucleic Acid Res. Mol. Biol.* **80**, 217–286.
27. Le Cam, E., Coulaud, D., Delain, E., Petitjean, P., Roques, B. P., Gerard, D. *et al.* (1998). Properties and growth mechanism of the ordered aggregation of a model RNA by the HIV-1 nucleocapsid protein: an electron microscopy investigation. *Biopolymers*, **45**, 217–229.

28. Mirambeau, G., Lyonnais, S., Coulaud, D., Hameau, L., Lafosse, S., Jeusset, J. *et al.* (2006). Transmission electron microscopy reveals an optimal HIV-1 nucleocapsid aggregation with single-stranded nucleic acids and the mature HIV-1 nucleocapsid protein. *J. Mol. Biol.* **364**, 496–511.
29. Stoylov, S. P., Vuilleumier, C., Stoylova, E., De Rocquigny, H., Roques, B. P., Gerard, D. & Mély, Y. (1997). Ordered aggregation of ribonucleic acids by the human immunodeficiency virus type 1 nucleocapsid protein. *Biopolymers*, **41**, 301–312.
30. Vo, M. N., Barany, G., Rouzina, I. & Musier-Forsyth, K. (2006). Mechanistic studies of mini-TAR RNA/DNA annealing in the absence and presence of HIV-1 nucleocapsid protein. *J. Mol. Biol.* **363**, 244–261.
31. Azoulay, J., Clamme, J. P., Darlix, J. L., Roques, B. P. & Mély, Y. (2003). Destabilization of the HIV-1 complementary sequence of TAR by the nucleocapsid protein through activation of conformational fluctuations. *J. Mol. Biol.* **326**, 691–700.
32. Beltz, H., Azoulay, J., Bernacchi, S., Clamme, J. P., Ficheux, D., Roques, B. *et al.* (2003). Impact of the terminal bulges of HIV-1 cTAR DNA on its stability and the destabilizing activity of the nucleocapsid protein NCp7. *J. Mol. Biol.* **328**, 95–108.
33. Beltz, H., Piemont, E., Schaub, E., Ficheux, D., Roques, B., Darlix, J. L. & Mély, Y. (2004). Role of the structure of the top half of HIV-1 cTAR DNA on the nucleic acid destabilizing activity of the nucleocapsid protein NCp7. *J. Mol. Biol.* **338**, 711–723.
34. Bernacchi, S., Stoylov, S., Piemont, E., Ficheux, D., Roques, B. P., Darlix, J. L. & Mély, Y. (2002). HIV-1 nucleocapsid protein activates transient melting of least stable parts of the secondary structure of TAR and its complementary sequence. *J. Mol. Biol.* **317**, 385–399.
35. Kankia, B. I., Barany, G. & Musier-Forsyth, K. (2005). Unfolding of DNA quadruplexes induced by HIV-1 nucleocapsid protein. *Nucleic Acids Res.* **33**, 4395–4403.
36. Urbaneja, M. A., Wu, M., Casas-Finet, J. R. & Karpel, R. L. (2002). HIV-1 nucleocapsid protein as a nucleic acid chaperone: spectroscopic study of its helix-destabilizing properties, structural binding specificity, and annealing activity. *J. Mol. Biol.* **318**, 749–764.
37. Williams, M. C., Gorelick, R. J. & Musier-Forsyth, K. (2002). Specific zinc-finger architecture required for HIV-1 nucleocapsid protein's nucleic acid chaperone function. *Proc. Natl Acad. Sci. USA*, **99**, 8614–8619.
38. Williams, M. C., Rouzina, I., Wenner, J. R., Gorelick, R. J., Musier-Forsyth, K. & Bloomfield, V. A. (2001). Mechanism for nucleic acid chaperone activity of HIV-1 nucleocapsid protein revealed by single molecule stretching. *Proc. Natl Acad. Sci. USA*, **98**, 6121–6126.
39. Anthony, R. M. & Destefano, J. J. (2007). *In vitro* synthesis of long DNA products in reactions with HIV-RT and nucleocapsid protein. *J. Mol. Biol.* **365**, 310–324.
40. Zuker, M. (2003). Mfold Web server for nucleic acid folding and hybridization prediction. *Nucleic Acids Res.* **31**, 3406–3415.
41. Liu, H. W., Cosa, G., Landes, C. F., Zeng, Y., Kovaleski, B. J., Mullen, D. G. *et al.* (2005). Single-molecule FRET studies of important intermediates in the nucleocapsid-protein-chaperoned minus-strand transfer step in HIV-1 reverse transcription. *Biophys. J.* **89**, 3470–3479.
42. Godet, J., de Rocquigny, H., Raja, C., Glasser, N., Ficheux, D., Darlix, J. L. & Mély, Y. (2006). During the early phase of HIV-1 DNA synthesis, nucleocapsid protein directs hybridization of the TAR complementary sequences *via* the ends of their double-stranded stem. *J. Mol. Biol.* **356**, 1180–1192.
43. Liu, H. W., Zeng, Y., Landes, C. F., Kim, Y. J., Zhu, Y., Ma, X. *et al.* (2007). Insights on the role of nucleic acid/protein interactions in chaperoned nucleic acid rearrangements of HIV-1 reverse transcription. *Proc. Natl Acad. Sci. USA*, **104**, 5261–5267.
44. Cantor, C. R. & Schimmel, P. R. (1980). *Biophysical Chemistry: Part III. The Behavior of Biological Macromolecules.* W. H. Freeman & Co., San Francisco, CA.
45. Shubsda, M. F., McPike, M. P., Goodisman, J. & Dabrowiak, J. C. (1999). Monomer–dimer equilibrium constants of RNA in the dimer initiation site of human immunodeficiency virus type 1. *Biochemistry*, **38**, 10147–10157.
46. Vo, M.-N., Barany, G., Rouzina, I. & Musier-Forsyth, K. (2009). Effect of Mg^{2+} and Na^{+} on the nucleic acid chaperone activity of HIV-1 nucleocapsid protein: Implications for reverse transcription. *J. Mol. Biol.* **386**, 773–788.
47. Dib-Hajj, F., Khan, R. & Giedroc, D. P. (1993). Retroviral nucleocapsid proteins possess potent nucleic acid strand renaturation activity. *Protein Sci.* **2**, 231–243.
48. Lapadat-Tapolsky, M., De Rocquigny, H., Van Gent, D., Roques, B., Plasterk, R. & Darlix, J. L. (1993). Interactions between HIV-1 nucleocapsid protein and viral DNA may have important functions in the viral life cycle. *Nucleic Acids Res.* **21**, 831–839.
49. Fisher, R. J., Rein, A., Fivash, M., Urbaneja, M. A., Casas-Finet, J. R., Medaglia, M. & Henderson, L. E. (1998). Sequence-specific binding of human immunodeficiency virus type 1 nucleocapsid protein to short oligonucleotides. *J. Virol.* **72**, 1902–1909.
50. Urbaneja, M. A., Kane, B. P., Johnson, D. G., Gorelick, R. J., Henderson, L. E. & Casas-Finet, J. R. (1999). Binding properties of the human immunodeficiency virus type 1 nucleocapsid protein p7 to a model RNA: elucidation of the structural determinants for function. *J. Mol. Biol.* **287**, 59–75.
51. Markham, N. R. & Zuker, M. (2005). DINAMelt Web server for nucleic acid melting prediction. *Nucleic Acids Res.* **33**, W577–W581.
52. Ramalanjaona, N., de Rocquigny, H., Millet, A., Ficheux, D., Darlix, J. L. & Mély, Y. (2007). Investigating the mechanism of the nucleocapsid protein chaperoning of the second strand transfer during HIV-1 DNA synthesis. *J. Mol. Biol.* **379**, 1041–1053.
53. Galetto, R. & Negroni, M. (2005). Mechanistic features of recombination in HIV. *AIDS Rev.* **7**, 92–102.
54. Gao, L., Balakrishnan, M., Roques, B. P. & Bambara, R. A. (2007). Insights into the multiple roles of pausing in HIV-1 reverse transcriptase-promoted strand transfers. *J. Biol. Chem.* **282**, 6222–6231.
55. Mirambeau, G., Lyonnais, S., Coulaud, D., Hameau, L., Lafosse, S., Jeusset, J. *et al.* (2007). HIV-1 protease and reverse transcriptase control the architecture of their nucleocapsid partner. *PLoS ONE*, **2**, e669.